Aspect ratio of bubbles in different liquid media: a novel correlation

Giorgio Besagni*[1,2], Niels G. Deen[2]

[1]Politecnico di Milano, Department of Energy, Via Lambruschini 4a, 20156 Milano, Italy

[1]Power & Flow Group, Department of Mechanical Engineering, Eindhoven University of Technology, P.O. Box 513, 5600 MB Eindhoven, Netherlands

[*] Corresponding author: Giorgio Besagni, giorgio.besagni@polimi.it, Politecnico di Milano, Department of Energy, Via Lambruschini 4a, 20156 Milano, Italy

Abstract

The bubble shape is a required parameter in the modeling and design of multiphase reactors. This communication contributes to the broader discussion and closes the knowledge gap by providing a practical correlation for the bubble shape. The correlation is based on a very large experimental dataset, encompassing a wide range of *Morton* numbers ($Log_{10}(Mo)$ in the range of - 10.8 and 2.3), flow conditions (single bubbles and dense bubbly flows) and considering both gravity-driven flows and flows with an extra-external pressure gradient (counter-current flows). The experimental data were post-processed to derive a simple and physics-based correlation, relating the bubble aspect ratio to the bubble *Reynolds* and *Eötvös* numbers. This correlation provides a more accurate description and covers a wider range of applicability compared with literature correlations. As such, it can be helpful in the estimation of the interfacial area and velocity of a dispersed phase rising in a continuous phase.

Keywords. Bubble column; Correlation; Bubble size; Bubble shape

Nomenclature

Abbreviations

MEG	Monoethylene glycol
NaCl	Sodium chloride

Non-dimensional parameters

$Eo = \dfrac{g(\rho_L - \rho_G)d_{eq}^2}{\sigma}$	Eötvös number	$[-]$
$Fr = \dfrac{v^2}{g d_{eq}}$	Froude number	$[-]$
$Mo = \dfrac{g(\rho_L - \rho_G)\mu_L^4}{\rho_L^2 \sigma^3}$	Morton number	$[-]$
$N_{\mu_r} = \dfrac{\mu_L}{\mu_G}$	Viscosity number	$[-]$
$Re = \dfrac{\rho_L v d_{eq}}{\mu_L}$	Reynolds number	$[-]$
$Ta = ReMo^{0.23}$	Tadaki number	$[-]$
$We = \dfrac{d_{eq} v^2 \rho_L}{\sigma}$	Weber number	$[-]$
$\Omega = Eo^a Re^b$	Aoyama number	$[-]$
$\Omega = EoRe$	Non-dimensional parameter in Eq. (18)	$[-]$

Symbols

a	Exponent in Eq. (6)	$[-]$
b	Exponent in Eq. (6)	$[-]$
d_c	Diameter of the column	$[m]$
d_{eq}	Bubble equivalent diameter	$[m]$

d_o	Gas sparger holes diameter	[mm]
E	Aspect ratio	$[-]$
n_{tot}	Total number of paremeters in Eq. (12)	$[-]$
p	Pressure	[Pa]
T	Temperature	[K]
X	Bubble minor axis	[mm]
y	Bubble major axis	[mm]
α	Exponent in aspect ratio correlation	$[-]$
ρ	Density	$[kg/m^3]$
g	Gravity acceleration	$[m/s^2]$
v	Bubble velocity	$[m/s]$
θ	Non-dimensional parameter	$[-]$
μ	Dynamic viscosity	$[Pa \cdot s]$
σ	Surface tension	$[N/m]$

Subscripts

L	Liquid phase
G	Gas phase

1 Introduction

The dispersion of gases into liquid phases gives rise to fascinating fluid dynamics phenomena, classified as "*bubbly flows*" when characterized by "*non-coalesce-induced structures*" (Besagni et al., 2018; Montoya et al., 2016). This type of multiphase flows characterizes the flow phenomena of multiphase reactors in the nuclear, the chemical and the process industries. The physical understanding of "*bubbly flows*", essential in reactors design and operation, can be achieved by unveiling the connections between the different fluid dynamic scales, e.g., the "*large-scale*" phenomena are imposed by the "*local-scale*" (Liang-Shih and Tsuchiya, 2013; Mudde, 2005). From a theoretical point of view, the "*local-scale*" might be defined by the simultaneous knowledge of three parameters: (i) the local void fraction; (ii) the local liquid velocity; (iii) the bubble size and shape. The lack of knowledge regarding the connection between these parameters is a bottleneck in defining general criteria for multiphase reactor design and operation. This communication addresses a precise question: is there a physics-based relationship to describe the bubble shape? The importance of this relationship is made evident by considering how the bubble shape affects the flow of the dispersed phase (i.e., drag and lift models require details on the bubble shape), the phenomena at the "*large-scale*" as well as the heat and mass transfer (Ziegenhein and Lucas, 2017). The baseline case to start the discussion concerns a single bubble rising into a stagnant liquid phase (viz. neglecting the interactions between bubbles) under the only action of gravity (viz., neglecting external effects); if considering a pure liquid phase and neglecting the gas density and the gas viscosity, the bubble shape depends on five physical parameters, leading to two independent non-dimensional parameters (Risso, 2018). The two parameters are generally selected out of the Reynolds (eq. (1)), the Eötvös (Eq. (2)), the Morton (Eq. (3)) and the Weber (Eq. (4)) numbers, defined at the "*bubble-scale*":

$$Re = \frac{\rho_L v d_{eq}}{\mu_L} \tag{1}$$

$$Eo = \frac{(\rho_L - \rho_G) g d_{eq}^2}{\sigma} \tag{2}$$

$$Mo = \frac{(\rho_L - \rho_G) g \mu_L^4}{\rho^2 \sigma^3} \tag{3}$$

$$We = \frac{\rho_L v^2 d_{eq}}{\sigma} \tag{4}$$

Eqs. (1-4) consider the sphere-equivalent bubble size (d_{eq}) and, thus, an analytical relationship between the bubble shape and above parameters can be interpreted as a relationship between the bubble shape and d_{eq}. Eventually, other non-dimensional parameters can be obtained by combining these four groups. Tadaki and Maeda (1961) proposed the Tadaki number, defined as follows:

$$Ta = ReMo^{0.23} \tag{5}$$

Aoyama et al. (Aoyama et al., 2016; Aoyama et al., 2018) proposed the following non-dimensional parameter:

$$\Omega = Eo^{a}Re^{b} \tag{6}$$

Other authors also mentioned the Froude number (Wellek et al., 1966):

$$Fr = \frac{v^2}{gd_{eq}} \tag{7}$$

Finally, if considering the gas properties, additional parameters are needed (Wellek et al., 1966), as Eq. (8):

$$N_{\mu_r} = \frac{\mu_L}{\mu_G} \tag{8}$$

It is known that the non-dimensional parameters are not independent of each other, as unveiled by the graphical representation proposed by Grace et al. (1976). In this perspective, Tomiyama (2004) discussed the physical interpretation of the non-dimensional parameters (i.e., forces acting on the boundary of the bubbles, surface forces, …), which provides a physical interpretation of the "*bubble shape regimes*" displayed in the Grace et al. (1976) diagram. In this perspective, *We* accounts for the inertial and the surface tension forces, *Eo* accounts for the buoyant and the surface tension forces and *Re* accounts for the inertial and viscous forces.

Coming back to the primary research question, even considering the baseline case of a single bubble, an analytical relationship between bubble shape and size is elusive so far. This lack of knowledge is far more severe when considering relevant operating conditions in the dense bubbly flows (Tian et al., 2019). A generally employed strategy is made of two steps. First, single rising bubbles are considered and the bubble shape is modelled by the aspect ratio (Eq. (9), where x is the bubble minor axis and y is the bubble major axis, (Ziegenhein and Lucas, 2017)):

$$E = \frac{x}{y} \tag{9}$$

Second, the outcomes obtained for single bubbles are extended to other flow conditions, as discussed by Loth (2008) and Liu et al. (2015). This two-step approach is questionable as the flow conditions and the phase properties affect the bubble shape. For example, Besagni and Inzoli (Besagni and Inzoli, 2016, 2019) discussed the need of ad-hoc bubble shape correlations valid for dense bubbly flow conditions. A similar discussion was proposed by Ziegenhein and Lucas (2017), who studied the bubble shape in bubbly flows in different experimental setups and flow conditions. The influence of the gas holdup on the bubble shape was also pointed out in the dissertation of Roghair (Roghair, 2012). Other studies focus on bubble size/shape correlations, but relying on single rising bubbles, rather than dense bubble flow conditions (Aoyama et al., 2018; Celata et al., 2006; Liu et al., 2015; Sanada et al., 2008; Shi et al., 2018; Tian et al., 2019). Despite the intense research activities, no correlation relating bubble shape and size encompassing different phase properties, flow conditions and experimental setups is available; in particular, a general approach is use the Wellek et al. (Wellek et al., 1966) correlation, which was obtained for droplets in liquids. For example, the Wellek et al. (1966) correlation is employed in the lift force coefficient proposed by Tomiyama et al. (2002). This approach has been criticized by Shi et al. (Shi et al., 2018), when implementing the bubble shape correlation of Besagni and Inzoli (2017) into a numerical code.

Taking into account the state-of-the-art, developing a general correlation for bubble shape and size is a priority in the current research agenda. This communication covers this gap of knowledge by using a very large dataset. encompassing different phase properties and flow conditions, to derive a general, yet simple, physics-based correlation.

2 Dataset

A complete dataset has been gathered and it considers a broad range of experiments carried out at different flow conditions (Table 1, more than 150,000 data points). The dataset encompasses a wide range of Morton numbers ($Log_{10}(Mo)$ in the range of - 10.8 and 2.3), flow conditions (single rising bubbles and dense bubbly flows), experimental setups (different gas spargers with different opening size, d_o) and considers both gravity driven flows and two-phase flow with an external pressure gradient (i.e., counter-current flows). For every study, data regarding bubble aspect ratio (Eq. (7)) and bubble size (d_{eq}) have been collected along with the liquid phase properties. The ideal gas law has been used to compute the gas density at the midpoint positions (Besagni et al., 2017). Based on these data, the equivalent Re is derived following the correlation proposed by Tomiyama (2004).

Table 1. *The experimental dataset*

Reference	Flow conditions	Gas holdup [%]		Phases	Properties			$\log_{10}(Mo)$ [-]
		Min	Max		ρ [kg/m3]	μ [Pa·s]	σ [N/m]	
(Besagni and Inzoli, 2019)	Bubble column in batch mode	1.19%	7.23%	Air-water-ethanol (0.05%wt)	998.06	0.00096	0.072588	-10.665
	Bubble column in batch mode	0.99%	7.01%	Air-water	997.05	0.00089	0.071990	-10.781
	Bubble column in counter-current mode (UL = -0.066 m/s)	1.70%	10.71%	Air-water	997.05	0.00089	0.071990	-10.781
(Besagni and	Annular gap bubble column	2.89%	9.75%	Air-water	997.04	0.00089	0.071990	-10.781

Reference	Flow conditions	Gas holdup [%]		Phases	Properties			$\log_{10}(Mo)$ [-]
Inzoli, 2016)	in batch mode							
	Annular gap bubble column in counter-current mode (UL = -0.04 m/s)	3.62%	3.62%	Air-water	997.05	0.00089	0.071990	-10.781
(Besagni et al., 2017)	Bubble column in batch mode	1.22%	7.18%	Air-water-MEG (0.05 %wt)	997.16	0.00089	0.071500	-10.770
	Bubble column in batch mode	1.19%	7.32%	Air-water-MEG (0.1 %wt)	997.23	0.00089	0.071500	-10.768
	Bubble column in batch mode	1.09%	7.61%	Air-water-MEG (0.5 %wt)	997.80	0.00090	0.071300	-10.747
	Bubble column in batch mode	1.12%	7.95%	Air-water-MEG (1 %wt)	998.52	0.00091	0.071100	-10.721
	Bubble column in batch mode	1.15%	7.95%	Air-water-MEG (5 %wt)	1004.21	0.00101	0.069600	-10.520
	Bubble column in batch mode	1.12%	6.07%	Air-water-MEG (8 %wt)	1008.44	0.00109	0.068500	-10.371
	Bubble column in batch mode	0.99%	3.91%	Air-water-MEG (10 %wt)	1011.25	0.00115	0.067700	-10.270
	Bubble column in batch mode	0.96%	3.38%	Air-water-MEG (80 %wt)	1094.80	0.00797	0.050200	-6.546
(Besagni and Inzoli, 2017)	Bubble column in batch mode	2.41%	2.41%	Air-water-NaCl (0.02 mol/l)	997.79	0.00090	0.072067	-10.770
	Bubble column in batch mode	2.28%	2.28%	Air-water-NaCl (0.07 mol/l)	1000.04	0.00092	0.072299	-10.735
	Bubble column in batch mode	2.28%	2.28%	Air-water-NaCl (0.12 mol/l)	1002.29	0.00094	0.072532	-10.702
	Bubble column in batch mode	2.38%	2.38%	Air-water-NaCl (0.14 mol/l)	1003.35	0.00095	0.072642	-10.686
	Bubble column in batch mode	2.63%	2.63%	Air-water-NaCl (0.17 mol/l)	1004.57	0.00096	0.072767	-10.668
Besagni and Inzoli - Unpublished	Bubble column in batch mode (perforated plate with d_o = 0.5 mm)	0.79%	5.06%	Air-water	997.04	0.00089	0.071990	-10.781
Besagni and Inzoli - Unpublished	Bubble column in batch mode (perforated plate with d_o = 1 mm)	0.66%	1.96%	Air-water	997.04	0.00089	0.071990	-10.781
Besagni and Inzoli - Unpublished	Bubble column in batch mode (perforated plate needle gas sparger d_o = 0.5 mm)	0.77%	2.44%	Air-water	997.04	0.00089	0.071990	-10.781
(Tian et al., 2019)	Rising bubbles	--	--	Nitrogen-Silicon oil (T:323 K, P:0.1 MPa)	970.00	0.30000	0.020600	0.971
	Rising bubbles	--	--	Nitrogen-Silicon oil (T:323 K, P:0.1 MPa)	951.60	0.19200	0.019100	0.303
	Rising bubbles	--	--	Nitrogen-Silicon oil (T:373 K, P: 0.1 MPa)	921.00	0.09940	0.016500	-0.636
	Rising bubbles	--	--	Nitrogen-Silicon oil (T:373 K, P: 0.1 MPa)	890.40	0.05960	0.014300	-1.323
	Rising bubbles	--	--	Nitrogen-Silicon oil (T:473 K. P:0.1 MPa)	859.80	0.03590	0.012500	-2.014
	Rising bubbles	--	--	Nitrogen-Paraffin (T:293 K. P:0.1 Mpa)	880.10	0.41800	0.031000	1.057
(Aoyama et al., 2016)	Rising bubbles	--	--	Air-water-glycerol (62 %wt)	1155.00	0.00980	0.067000	-6.585
	Rising bubbles	--	--	Air-water-glycerol (70 %wt)	1178.00	0.01800	0.066700	-5.531
	Rising bubbles	--	--	Air-water-glycerol (75 %wt)	1191.00	0.02600	0.066600	-4.895
	Rising bubbles	--	--	Air-water-glycerol (80 %wt)	1204.00	0.04500	0.066200	-3.939
(Liu et al., 2015)	Rising bubbles	--	--	Air-water-glycerin (S1 case)	1246.10	0.62220	0.065000	0.633
	Rising bubbles	--	--	Air-water-glycerin (S2 case)	1236.00	0.30610	0.065000	-0.596
	Rising bubbles	--	--	Air-water-glycerin (S3 case)	1220.30	0.11530	0.066000	-2.307
	Rising bubbles	--	--	Air-water-glycerin (S4 case)	1206.50	0.06300	0.067000	-3.371
	Rising bubbles	--	--	Air-water (T = 8°C)	999.80	0.00138	0.074000	-10.057
	Rising bubbles	--	--	Air-water (T = 29°C)	996.70	0.00086	0.072000	-10.842
(Aoyama et al.,	Rising bubbles	--	--	Air-water-glycerol solution	1116.00	0.00440	0.069000	-7.999

Reference	Flow conditions	Gas holdup [%]		Phases	Properties			$\log_{10}(Mo)$ [-]
2018)				contaminated with Triton x-100 (0.2 mol/m3)				
	Rising bubbles	--	--	Air-water-glycerol solution contaminated with 1-Octanol (3.25 mol/m3)	1116.00	0.00440	0.069000	-7.999
	Rising bubbles	--	--	Air-water-glycerol solution contaminated with SDS (5 mol/m3)	1116.00	0.00440	0.069000	-7.999
	Rising bubbles	--	--	Air-water-glycerol solution contaminated with 1-Decanol (0.16 mol/m3)	1116.00	0.00440	0.069000	-7.999
	Rising bubbles	--	--	Air-water-glycerol solution contaminated with Triton x-100 (0.2 mol/m3)	1154.00	0.00930	0.068000	-6.695
	Rising bubbles	--	--	Air-water-glycerol solution contaminated with 1-Octanol (3.25 mol/m3)	1154.00	0.00930	0.068000	-6.695
	Rising bubbles	--	--	Air-water-glycerol solution contaminated with SDS (5 mol/m3)	1154.00	0.00930	0.068000	-6.695
	Rising bubbles	--	--	Air-water-glycerol solution contaminated with 1-Decanol (0.16 mol/m3)	1154.00	0.00930	0.068000	-6.695
	Rising bubbles	--	--	Air-water-glycerol solution contaminated with Triton x-100 (0.2 mol/m3)	1205.00	0.04670	0.067000	-3.891
	Rising bubbles	--	--	Air-water-glycerol solution contaminated with 1-Octanol (3.25 mol/m3)	1205.00	0.04670	0.067000	-3.891
	Rising bubbles	--	--	Air-water-glycerol solution contaminated with SDS (5 mol/m3)	1205.00	0.04670	0.067000	-3.891
	Rising bubbles	--	--	Air-water-glycerol solution contaminated with 1-Decanol (0.16 mol/m3)	1205.00	0.04670	0.067000	-3.891
(Ziegenhein and Lucas, 2017)	Bubble plume	0,34%	3,22%	Air-water	997.09	0.00089	0.071500	-10.773
	Airlift	2,35%	5,14%	Air-water	997.09	0.00089	0.071500	-10.773
	Rising bubbles (single needle esperiments)	--	--	Air-water	997.09	0.00089	0.071500	-10.773
	Rising bubbles (single bubble experiments)	--	--	Air-water	997.09	0.00089	0.071500	-10.773
(Seo et al., 2018)	Single rising bubbles with plain nozzle (2 l/min)	--	--	Air-water	997.09	0.00089	0.071500	-10.773
	Single rising bubbles with ejector (2 l/min))	--	--	Air-water	997.09	0.00089	0.071500	-10.773
	Single rising bubbles with ejector in co-flow (2 l/min)	--	--	Air-water	997.09	0.00089	0.071500	-10.773
	Single rising bubbles with plain nozzle (15 l/min)	--	--	Air-water	997.09	0.00089	0.071500	-10.773
	Single rising bubbles with ejector (15 l/min)	--	--	Air-water	997.09	0.00089	0.071500	-10.773
	Single rising bubbles with ejector in co-flow (15 l/min)	--	--	Air-water	997.09	0.00089	0.071500	-10.773
(Sanada et al., 2008)	Rising bubbles	--	--	Air-super-purified water	997.50	0.00094	0.072300	-10.694
(Cai et al., 2010)	Rising bubbles	--	--	Air-water	995.00	0.00106	0.072000	-10.478
	Rising bubbles	--	--	Air-water-glycerol (20 %vol)	1054.00	0.00948	0.056400	-6.378
	Rising bubbles	--	--	Air-water-glycerol (81.6 %vol)	1220.00	0.10500	0.060700	-2.360
	Rising bubbles	--	--	Air-water-glycerol (91.4 %vol)	1241.00	0.33800	0.061000	-0.343
	Rising bubbles	--	--	Air-water-glycerol (98.0 %vol)	1264.00	0.97200	0.060100	1.503
	Rising bubbles	--	--	Air-water-glycerol (100 %vol)	1265.00	1.51500	0.059000	2.298

Reference	Flow conditions	Gas holdup [%]		Phases	Properties			$\log_{10}(Mo)$ [-]
(Huang et al., 2018)	Rising bubbles	--	--	Carbon dioxide-turpentine	855.80	0.00100	0.028100	-9.288
	Rising bubbles	--	--	Carbon dioxide-pine resin: turpentine solution (1:3.75 mass ratio)	892.00	0.00280	0.031000	-7.645
	Rising bubbles	--	--	Carbon dioxide-pine resin: turpentine solution (1:3.00 mass ratio)	892.00	0.00280	0.030800	-7.637
	Rising bubbles	--	--	Carbon dioxide-pine resin: turpentine solution (1:2.25 mass ratio)	916.40	0.00690	0.030400	-6.065
	Rising bubbles	--	--	Carbon dioxide-pine resin: turpentine solution (1:1.5 mass ratio)	934.40	0.01250	0.030000	-5.024
(Celata et al., 2006)	Rising bubbles (d_o = 5 mm)	--	--	Air-contaminated water	998.00	0.00100	0.072000	-10.580
	Rising bubbles (d_o = 4 mm)	--	--	Air-contaminated water	998.00	0.00100	0.072000	-10.580
	Rising bubbles (d_o = 2.5 mm)	--	--	Air-contaminated water	998.00	0.00100	0.072000	-10.580
	Rising bubbles (d_o = 1.8 mm)	--	--	Air-contaminated water	998.00	0.00100	0.072000	-10.580
	Rising bubbles (d_o = 0.9 mm)	--	--	Air-contaminated water	998.00	0.00100	0.072000	-10.580
	Rising bubbles (d_o = 0.5 mm)	--	--	Air-contaminated water	998.00	0.00100	0.072000	-10.580
	Rising bubbles (d_o = 5 mm)	--	--	Air-pure water	998.00	0.00100	0.072000	-10.580
	Rising bubbles (d_o = 5 mm)	--	--	Air-commercial FC-72	1692.00	0.00069	0.012000	-9.119
	Rising bubbles (d_o = 5 mm)	--	--	Air-distilledl FC-72	1692.00	0.00069	0.012000	-9.119
	Rising bubbles (d_o = 0.9 mm)	--	--	Air-distilledl FC-72	1692.00	0.00069	0.012000	-9.119

3 Results and discussion

3.1 Proposed scheme of correlation

The bubble aspect ratio depends on the flow conditions, bubble size, bubble motion as well as the phase properties. Wellek et al. (1966), in their pioneering work, started their discussion considering the following determinants:

$$E = f\left(v, \sigma, d_{eq}, \mu_L, \mu_G, \rho_L, \rho_G, g\right) \tag{10}$$

Subsequently, they applied the dimensional analysis to derive the determinants expressed in Eq. (11):

$$E = f\left(\frac{d_{eq} v^2 \rho_L}{\sigma}, \frac{d_{eq} v \rho_L}{\mu_L}, \frac{(\rho_L - \rho_G) g d_{eq}^2}{\sigma}, \frac{v^2}{g d_{eq}}, \frac{\mu_L}{\mu_G}\right) = f\left(We, Re, Eo, Fr, N_{\mu_r}\right) \tag{11}$$

Eq. (11) belongs to a more general approach, which can be written as follows:

$$E = f(\theta_i)_{i=1}^{n_{tot}} \tag{12}$$

Where θ_i is a non-dimensional parameter and n_{tot} represents the numbers of non-dimensional parameters needed to characterize the system. The closure of the analytical problem relies on the formulation of the *f-function* in Eq. (12). For example, Wellek et al. (1966) proposed Eq. (13):

$$\frac{1}{E}-1=\alpha_0\prod_{i=1}^{n_{tot}}{\theta_i}^{\alpha_i}\xrightarrow{yields}\frac{1}{E}=1+\alpha_0\prod_{i=1}^{n_{tot}}{\theta_i}^{\alpha_i} \tag{13}$$

Subsequently, they computed the *α-coefficients* by a multiple regression approach: the statistical significance of the non-dimensional parameters was identified and, stating from a baseline case, additional contributions were considered. They concluded that including additional parameters does not provide advantages and, thus, a one-parameter correlation was used. As demonstrated in the following, this outcome cannot be applied in bubble shape correlations encompassing a broad range of *Mo* numbers. In this paper, instead of the Wellek et al. (1966) *f-function*, the approach of Aoyama et al. (2018) was followed, i.e.:

$$\frac{1}{E}=\left[1+\alpha_0\prod_{i=1}^{n_{tot}}{\theta_i}^{\alpha_1}\right]^{\alpha_{exp}} \tag{14}$$

It should be noted that Eq. (14) is a generalization of Eq. (13). At this point, a physics-based selection of ϑ_i parameters should be conducted. Aoyama et al. (2016, 2018) mentioned that existing correlations suffer from lack of accuracy when encompassing a broad range of *Mo* numbers. The reason for this observation is given in the supplementary material (*S1*), which collects a series of figures displaying the relationship between *Eo* and *E* for different *Mo* numbers; a distinct behavior between low- *Mo* and high- *Mo* systems is observed, which is in agreement with the bubble shape mapping proposed in the Grace diagram and which suggests a clear transition between two prevailing "*shape regimes*" (spherical and distorted). To address this concern, a general correlation should consider all the characteristic forces (viz., surface tension, buoyant, viscous and inertial forces). This is established by including effects related to the *Re* (ratio of inertial forces to viscous forces) and the *Eo* (ratio of the gravitational forces compared to surface tension forces) numbers. Note that the combination of *Eo* and *We* cannot be used as viscous forces would not be considered (and, thus, the dependency on the *Mo* number would not be considered). Hence, from Eq. (14) we derive Eq. (15):

$$\frac{1}{E}=\left[1+\alpha_0\prod_{i=1}^{n_{tot}}{\theta_i}^{\alpha_1}\right]^{\alpha_{exp}}\xrightarrow{yields}\frac{1}{E}=\left[1+\alpha_0\left({\theta_1}^{\alpha_1}{\theta_2}^{\alpha_2}\right)\right]^{\alpha_{exp}} \xrightarrow{yields}\frac{1}{E}=\left[1+\alpha_0\left(Eo^{\alpha_1}Re^{\alpha_1}\right)\right]^{\alpha_{exp}} \tag{15}$$

Eq. (15) also writes as follows:

$$E=\frac{1}{\left[1+\alpha_0\left(Eo^{\alpha_1}Re^{\alpha_2}\right)\right]^{\alpha_{exp}}} \tag{16}$$

The *α-coefficients* in Eq. (16) are computed by testing Eq. (16) against all data (the comparison is performed for the different *Mo* numbers) and applying the least squares estimation. Based on this approach, Eq. (17) is obtained:

$$E = \frac{1}{(1 + 0.4Eo^{1.19}Re^{1.05})^{0.07}} \tag{17}$$

Given the structure of Eq. (17), the exponents of *Eo* an *Re* can be forced to unity, without significant loss in terms of the predictively capability. This changes the functional form into:

$$E = \frac{1}{[1 + 0.45(EoRe)]^{0.08}} \xrightarrow{\chi = ReEo} \frac{1}{[1 + 0.45\chi]^{0.08}} \tag{18}$$

Eq. (18) accounts for all the characteristics forces, simultaneously and with the same exponents. For small *Eo* and/or *Re* the aspect ratio tends to unity: for small *Eo* bubbles become spherical due to dominating surface forces, whereas for small *Re* bubbles become spherical due dominating viscous forces. Conversely, at higher *Eo* and/or *Re* values, the aspect ratio decreases (viz., aspect ratio is in the range of 0.6 - 0.4, when χ is in the range of $10^4 - 10^5$). Peculiar behavior of the data is observed for *Mo* in the range of 1.5 10^{-11} and 10^{-10}: in this situation, the aspect ratio decreases to 0.5 when χ is in the range of $10^4 - 10^5$ and, subsequently, it increases again up to 0.6 - 0.7 when χ is in the range of $10^5 - 2{\cdot}10^6$. These data were obtained by Besagni and Inzoli (Table 1) in a large-scale bubble column operated either in different operation modes (batch mode or counter-current mode), in different system configurations and with different gas spargers. As their studies considered dense bubbly flow conditions, these observations suggest that the high gas holdup (in high-χ range conditions) have a positive effect of the bubble aspect ratio. This outcome is somehow in agreement with the outcomes of the work of Roghair (2012). Unfortunately, there is a severe lack of experimental studies focused on the high-χ range at different *Mo* numbers, so that the validity of this statement should be verified in future work. For the sake of clarity, the supplementary material (*S2*) proposes figures comparing single bubble and dense bubbly flow conditions.

Figure 1 compares the present correlation against the whole dataset (for the sake of clarity, the results are grouped according to *Mo*), showing fair agreement in the complete range. The Grace diagram shown in Figure 2 shows iso-E curves, i.e. the skewed lines with constant values of *EoRe*. These iso-E curves appear to indicate the boundaries of the different bubble rise regimes. This is best seen for the iso-E line at which *EoRe* ≈ 0.7 bubbles. For all gas-liquid systems, identified by the Morton number, there is a change in slope related to bubbles changing shape from spherical to non-spherical. The more accurate description as well as the higher generality of Eq. (18) compared with previous literature correlations will be demonstrated in the forthcoming section.

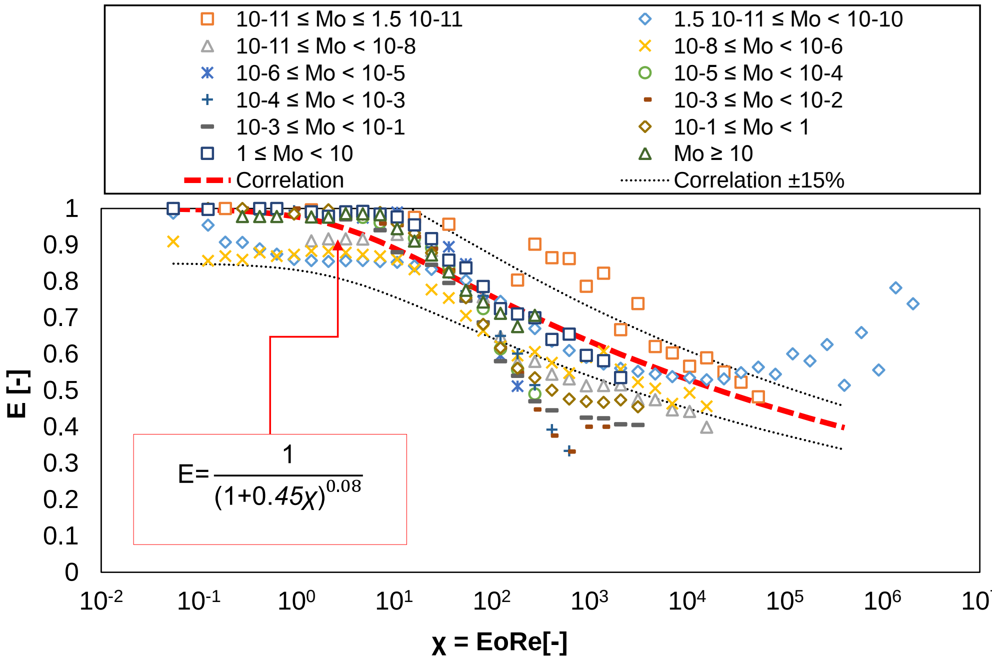

Figure 1. Comparison between the newly proposed correlation for bubble aspect ratio (Eq. 18) and the experimental data (Table 1).

3.2 Literature correlations

This section reports the predictive capability of literature correlations against the dataset summarized in Table 1. First, correlations employing a single non-dimensional parameter are considered; subsequently, two-parameter correlations are tested. Figure 3 considers *Eo*-based correlations (Besagni and Inzoli, 2016; Moore, 1965; Sugihara et al., 2007; Wellek et al., 1966) and Figure 4 considers the We based correlations (Moore, 1965; Sugihara et al., 2007). Figure 5 considers *Ta*-based correlations (Fan and Tsuchiya, 1990; Myint et al., 2007; Tadaki and Maeda, 1961) and, finally, Figure 6 focuses on the Aoyama et al. (2016) correlation.

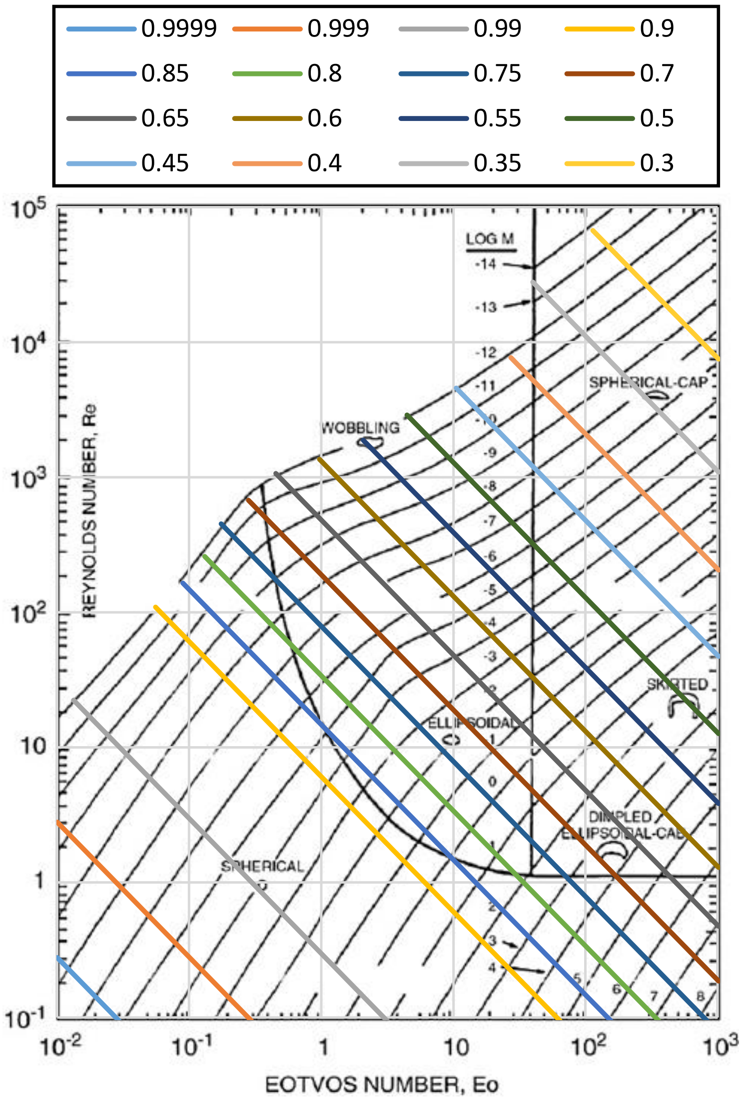

Figure 2. Iso-*E* lines of constant *EoRe* (Eq. 18) plotted on the Grace diagram.

Considering *Eo*-based correlations, the pioneering equation of Wellek et al. (1966) should be mentioned first. It was developed for droplets in contaminated liquids (yet, some authors stated that it may be applied to bubbles in low viscous systems (Fan and Tsuchiya, 1990)):

$$E = \frac{1}{1 + 0.163Eo^{0.757}} \tag{19}$$

Variations to the correlation of Wellek et al. (1966) were suggested by Okawa et al. (2003) (Eq. 20), to fit the lower boundary of their data, by Sugihara et al. (2007) (Eq. 21) and, finally, by Besagni and Inzoli (2016) (Eq. 22), to fit their data obtained in an annular gap bubble column (considered within Table 1 data).

$$E = \frac{1}{1 + 1.97Eo^{1.3}} \tag{20}$$

$$E = \frac{1}{1 + 6.5Eo^{1.925}} \tag{21}$$

$$E = \frac{1}{1 + 0.553Eo^{0.266}} \tag{22}$$

None of the *Eo*-based correlations are able to predict the entire range of *Mo* numbers. This conclusion was expected as bubble shape depends on all forces acting on bubbles, while *Eo* only considers buoyant and surface forces. This concept is made clear by looking at the predictive capability of the correlation of Besagni and Inzoli (2016). It is able to fit fairly well the low-*Mo* systems, but fails in the other cases. For this reason, these correlations may be used as first approximation for air-water systems (i.e., to replace the Wellek et al. (1966) correlation within the Tomiyama lift force coefficients in numerical simulations (Shi et al., 2018)).

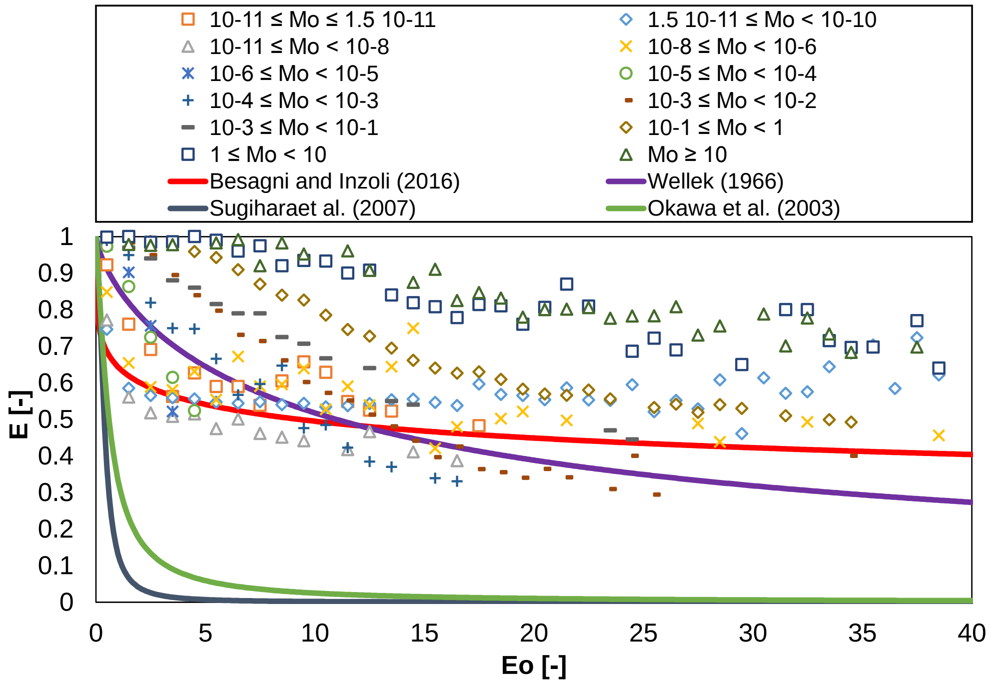

Figure 3. Comparison between Eo-based correlations and the experimental data (Table 1).

Another set of correlations is based on *We* number, which considers the inertial and viscous forces. Moore (1965) formulated a complex relationship between *E* and *We*, which can be simplified (assuming small shape deformation), as follows:

$$E = \frac{1}{1 + \frac{9}{64}We} \tag{23}$$

Eq. (23) was generalized by Sugihara et al. (2007), by including an additional contribution:

$$E = \frac{1}{1 + \frac{9}{64}We + \frac{0.04We^2}{(3.7 - We)^{0.5}}} \qquad (24)$$

It is found that Eq. (23) and (24) are able to model low-Mo systems at low-We numbers, but they fail in other cases. As expected, Eq. (24) improves the predictive capability of Eq. (23). As mentioned for the Eo-based correlations, the use of a single non-dimensional parameter is the main cause of the lack of generality of these correlations. This can be cured by considering an additional dimensionless group, such as the Tadaki number, which is the combination of Re and Mo or the Ω parameter of Aoyama et al. (2016).

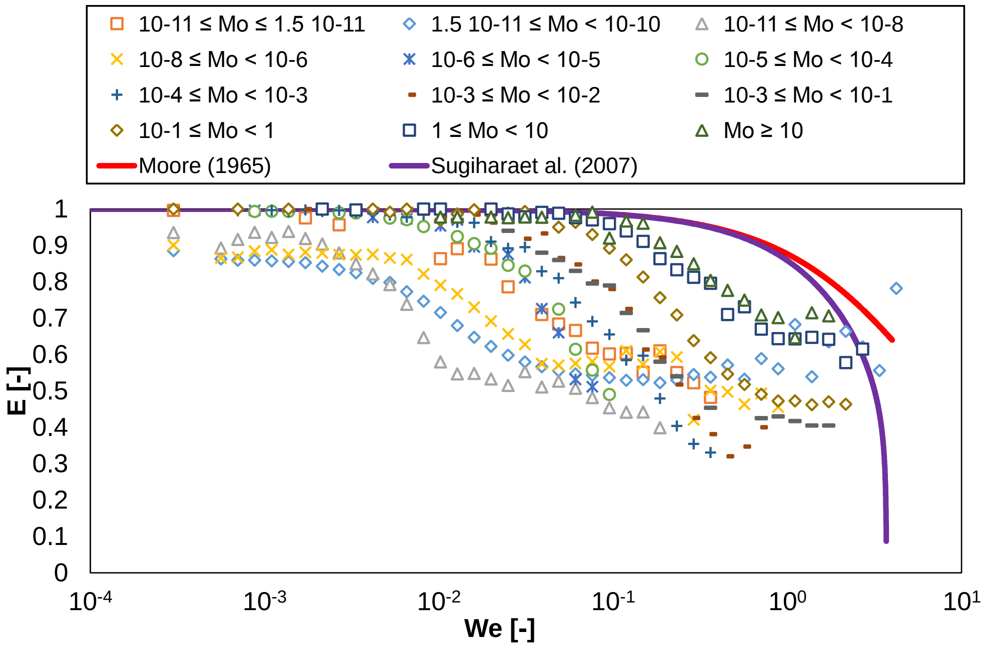

Figure 4. Comparison between We-based correlations and the experimental data (Table 1).

Regarding *Ta*-based correlations, Tadaki and Maeda (1961) (Eq. (25)) proposed a correlation for bubbles in low-Morton systems, Myint et al. (2007) (eq. (26) proposed a correlation for droplets in stagnant liquids and, finally, Fan and Tsuchiya (1990) (Eq. (27) modified a previous correlation (Vakrushev I.A, 1970) to make it suitable for clean bubbles:

$$E^{1/3} = \begin{cases} 0.62 & 16.5 < Ta \\ 1.36Ta^{-0.28} & 6 < Ta \leq 16.5 \\ 1.14Ta^{-0.176} & 2 < Ta \leq 6 \\ 1 & Ta \leq 2 \end{cases} \qquad (25)$$

$$E = 1 - 0.0487Ta - 0.0289Ta^2 \qquad (26)$$

$$E = \begin{cases} 0.24 & Ta \geq 39.8 \\ \{0.81 + 0.206 \tanh[2(0.8 - log10\, Ta)]\}^3 & 1 < Ta \leq 39.8 \\ 1 & Ta \leq 1 \end{cases} \quad (27)$$

Aoyama et al. (2016) used the combination of Re and Eo numbers to consider all the effects of the various forces on E:

$$E = \frac{1}{[1 + 0.016(Eo^{1.12}Re)]^{0.388}} \quad (28)$$

All above equations (Eqs. (25-28)), were compared with the current dataset. Although all these correlations outperform the single parameter correlations discussed in the previous section (Figures 5 and 6), it turns out the newly proposed correlation, owing to the broader range of calibration, has a better generality (viz., a broader range of application) and is considered a clear advancement compared with the existing body of knowledge.

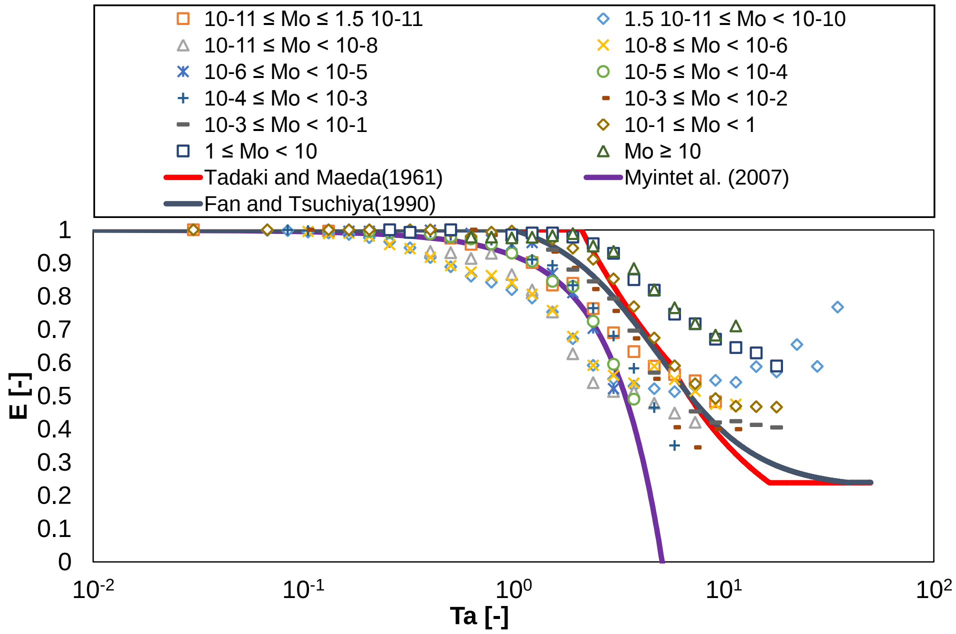

Figure 5. Comparison between Ta-based correlations and the experimental data (Table 1).

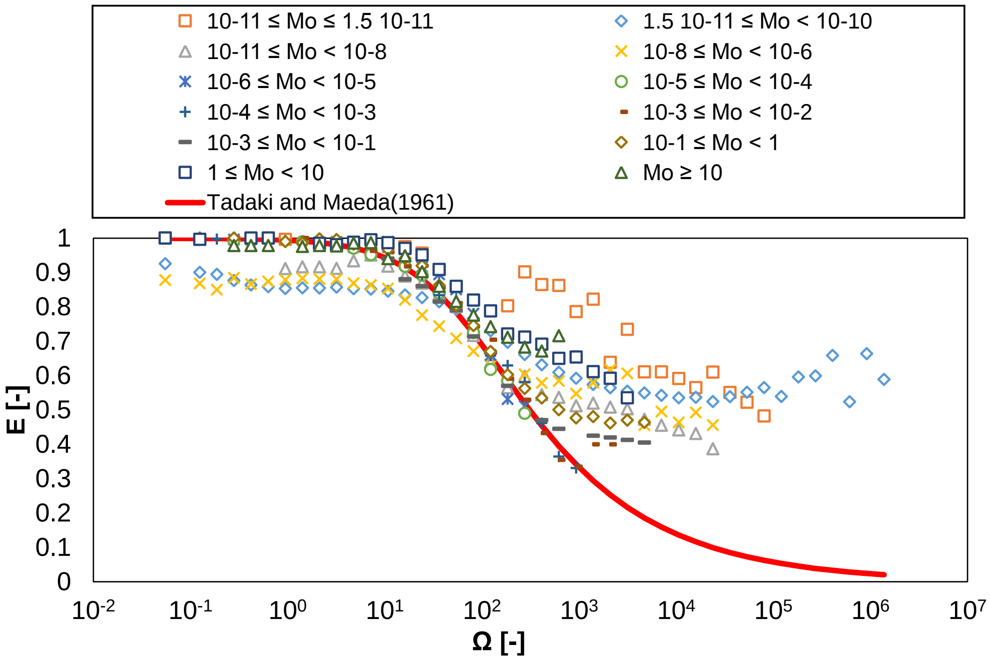

Figure 6. Comparison between the Aoyama number based correlation and the experimental data (Table 1).

4 Conclusions

A precise understanding of multiphase flows in multiphase reactors relies on the precise prediction of the local-scale flow parameters. This short communication focuses on a specific lack of knowledge: correlations to relate bubble shape to dimensionless groups of the bubble. Based on a comprehensive dataset (encompassing a wide range of *Mo* numbers, flow conditions and experimental setups) a novel correlation is proposed. The proposed correlation is based on two non-dimensional parameters (*Re* and *Eo*) to account for all forces determining and influencing the bubble shape (viz., surface tension, buoyant, viscous and inertial forces). Its structure is simple in its formulation and general in its range of applications. Subsequently, previously proposed correlations have been applied to the same experimental dataset, showing lower performances compared with the novel correlation. In conclusion, this communication provides engineers and researchers a practical physics based tool that can be helpful in the estimation of the interfacial area, and slip velocity of dispersed rising bubbles. Future studies will be devoted to extend the proposed correlation to take into account swarm effects; to this end, extensive experimental studies are needed to cover the lack of data regarding bubble shapes at low/intermediate gas holdup. Future studies should also extend the proposed correlation considering interfacial properties, flow phenomena nearby bubbles and/or induced by bubbles themselves (i.e., bubble wake effects).

5 REFERENCES

Aoyama, S., Hayashi, K., Hosokawa, S., Tomiyama, A., 2016. Shapes of ellipsoidal bubbles in infinite stagnant liquids. International Journal of Multiphase Flow 79, 23-30.

Aoyama, S., Hayashi, K., Hosokawa, S., Tomiyama, A., 2018. Shapes of single bubbles in infinite stagnant liquids contaminated with surfactant. Experimental Thermal and Fluid Science 96, 460-469.

Besagni, G., Inzoli, F., 2016. Bubble size distributions and shapes in annular gap bubble column. Experimental Thermal and Fluid Science 74, 27-48.

Besagni, G., Inzoli, F., 2017. The effect of electrolyte concentration on counter-current gas–liquid bubble column fluid dynamics: Gas holdup, flow regime transition and bubble size distributions. Chemical Engineering Research and Design 118, 170-193.

Besagni, G., Inzoli, F., 2019. Bubble sizes and shapes in a counter-current bubble column with pure and binary liquid phases. Flow Measurement and Instrumentation 67, 55-82.

Besagni, G., Inzoli, F., De Guido, G., Pellegrini, L.A., 2017. The dual effect of viscosity on bubble column hydrodynamics. Chemical Engineering Science 158, 509-538.

Besagni, G., Inzoli, F., Ziegenhein, T., 2018. Two-phase bubble columns: A comprehensive review. ChemEngineering 2(2), 13.

Cai, Z., Bao, Y., Gao, Z., 2010. Hydrodynamic Behavior of a Single Bubble Rising in Viscous Liquids. Chinese Journal of Chemical Engineering 18(6), 923-930.

Celata, G.P., Cumo, M., D'Annibale, F., Di Marco, P., Tomiyama, A., Zovini, C., 2006. Effect of gas injection mode and purity of liquid on bubble rising in two-component systems. Experimental Thermal and Fluid Science 31(1), 37-53.

Fan, L.S., Tsuchiya, K., 1990. Bubble Wake Dynamics in Liquids and Liquid-Solid Suspensions. Butterworth-Heinemann, Oxford.

Grace, J.R., Wairegi, T. & Nguyen, T. H., 1976. Shapes and Velocities of Single Drops and Bubbles Moving Freely Through Immiscible Liquids. Transactions of the Institute of the Chemical Engineers 54, 167.

Huang, C., Wang, L., Chen, X., Wei, X., Liang, J., 2018. The rising behaviors of single bubbles in stagnant turpentine and pine resin solutions. Experimental Thermal and Fluid Science 98, 170-180.

Liang-Shih, F., Tsuchiya, K., 2013. Bubble wake dynamics in liquids and liquid-solid suspensions. Butterworth-Heinemann.

Liu, L., Yan, H., Zhao, G., 2015. Experimental studies on the shape and motion of air bubbles in viscous liquids. Experimental Thermal and Fluid Science 62, 109-121.

Loth, E., 2008. Quasi-steady shape and drag of deformable bubbles and drops. International Journal of Multiphase Flow 34(6), 523-546.

Montoya, G., Lucas, D., Baglietto, E., Liao, Y., 2016. A review on mechanisms and models for the churn-turbulent flow regime. Chemical Engineering Science 141, 86-103.

Moore, D.W., 1965. The velocity of rise of distorted gas bubbles in a liquid of small viscosity. Journal of Fluid Mechanics 23(4), 749-766.

Mudde, R.F., 2005. Gravity-driven bubbly flows. Annual Review of Fluid Mechanics 37(1), 393-423.

Myint, W., Hosokawa, S., Tomiyama, A., 2007. Shapes of Single Drops Rising Through Stagnant Liquids. Journal of Fluid Science and Technology 2(1), 184-195.

Risso, F., 2018. Agitation, Mixing, and Transfers Induced by Bubbles. Annual Review of Fluid Mechanics 50(1), 25-48.

Roghair, I., 2012. Direct numerical simulations of hydrodynamics and mass transfer in dense bubbly flows. Technische Universiteit Eindhoven.

Sanada, T., Sugihara, K., Shirota, M., Watanabe, M., 2008. Motion and drag of a single bubble in super-purified water. Fluid Dynamics Research 40(7), 534-545.

Seo, H., Aliyu, A.M., Kim, K.C., 2018. Enhancement of momentum transfer of bubble swarms using an ejector with water injection. Energy 162, 892-909.

Shi, W., Yang, J., Li, G., Yang, X., Zong, Y., Cai, X., 2018. Modelling of breakage rate and bubble size distribution in bubble columns accounting for bubble shape variations. Chemical Engineering Science 187, 391-405.

Sugihara, K., Sanada, T., Shirota, M., Watanabe, M., 2007. Behavior of Single Rising Bubbles in Superpurified Water. KAGAKU KOGAKU RONBUNSHU 33(5), 402-408.

Tadaki, T., Maeda, S., 1961. On the Shape and Velocity of Single Air Bubbles Rising in Various Liquids. Chemical engineering 25(4), 254-264.

Tian, Z., Cheng, Y., Li, X., Wang, L., 2019. Bubble shape and rising velocity in viscous liquids at high temperature and pressure. Experimental Thermal and Fluid Science 102, 528-538.

Tomiyama, A., 2004. Drag, lift and virtual mass forces acting on a single bubble, In 3rd Int. Symp. Two-Phase Flow Modeling and Experimentation Pisa.

Tomiyama, A., Tamai, H., Zun, I., Hosokawa, S., 2002. Transverse migration of single bubbles in simple shear flows. Chemical Engineering Science 57(11), 1849-1858.

Vakrushev I.A, E.G.I., 1970. The velocities of single gas bubbles in liquids. Chem. Technol. Fuels Oils (USSR) 5/6, 376-379.

Wellek, R.M., Agrawal, A.K., Skelland, A.H.P., 1966. Shape of liquid drops moving in liquid media. AIChE Journal 12(5), 854-862.

Ziegenhein, T., Lucas, D., 2017. Observations on bubble shapes in bubble columns under different flow conditions. Experimental Thermal and Fluid Science 85, 248-256.